Supplemental Information

Global dynamics of non-equilibrium gliding in animals

Isaac J. Yeaton[1,*], John J. Socha[2] and Shane D. Ross[2]

[1]Department of Mechanical Engineering
[2]Department of Biomedical Engineering and Mechanics
Virginia Tech
[*]Corresponding author: iyeaton@vt.edu

March 1, 2017

Code repository

Python code to reproduce figures in the manuscript, including velocity polar diagrams and pitch bifurcation diagrams, can be found at
`https://github.com/TheSochaLab/Global-dynamics-of-non-equilibrium-gliding-in-animals`.

1 Linear stability analysis

The Jacobian of the polar coordinate equations (2.7) and (2.8) in the main text, evaluated at equilibrium is

$$A_{(\gamma^*,\hat{v}^*)} = \begin{bmatrix} \dfrac{\partial \gamma'}{\partial \gamma} & \dfrac{\partial \gamma'}{\partial \hat{v}} \\ \dfrac{\partial \hat{v}'}{\partial \gamma} & \dfrac{\partial \hat{v}'}{\partial \hat{v}} \end{bmatrix}_{(\gamma^*,\hat{v}^*)} \tag{1.1}$$

After simplification, the partial derivatives are

$$\frac{\partial \gamma'}{\partial \gamma} = -\frac{(C_L' + C_D)}{(C_L^2 + C_D^2)^{1/4}} \qquad \frac{\partial \gamma'}{\partial \hat{v}} = -2C_L$$
$$\frac{\partial \hat{v}'}{\partial \gamma} = \frac{C_L - C_D'}{(C_L^2 + C_D^2)^{1/2}} \qquad \frac{\partial \hat{v}'}{\partial \hat{v}} = \frac{-2C_D}{(C_L^2 + C_D^2)^{1/4}}$$

where the lift and drag coefficient values, as well as their slopes C_L' and C_D', are evaluated at the equilibrium angle of attack in radians.

Common types of equilibrium points can be calculated analytically. Saddle point equilibria occur when

$$(C_L/C_D)' < -\left[1 + (C_L/C_D)^2\right]$$

and stable equilibria occur when

$$C_L' > -3C_D.$$

Lastly, the equilibrium glide velocities at any equilibrium are

$$\hat{v}^* = (C_L^2 + C_D^2)^{-1/4} \qquad \hat{v}_x^* = \hat{v}^* \cos\gamma^* \qquad \hat{v}_z^* = -\hat{v}^* \sin\gamma^*. \tag{1.2}$$

2 Conversion between dimensional, non-dimensional, and rescaled quantities

Below we list the conversion from dimensional quantities, non-dimensional quantities (with the overbar), and rescaled quantities (with an overhat).

$$t = \sqrt{\frac{c}{g\epsilon}}\hat{t} \qquad x = \frac{c}{\epsilon}\hat{x} \qquad v = \sqrt{\frac{cg}{\epsilon}}\hat{v} \qquad a = g\hat{a} \tag{2.1}$$

$$t = \sqrt{\frac{c}{g}}\bar{t} \qquad x = c\bar{x} \qquad v = \sqrt{cg}\bar{v} \qquad a = g\bar{a} \tag{2.2}$$

$$\bar{t} = \frac{\hat{t}}{\sqrt{\epsilon}} \qquad \bar{x} = \frac{\hat{x}}{\epsilon} \qquad \bar{v} = \frac{\hat{v}}{\sqrt{\epsilon}} \qquad \bar{a} = \hat{a} \tag{2.3}$$

The universal glide scaling parameter,

$$\epsilon = \frac{\rho c}{2}\frac{S}{m} = \frac{\rho g}{2}\frac{c}{W_S} \tag{2.4}$$

when substituted back into the rescaled terms, results in the wing loading expression in the main text (equation 4.1):

$$t = \sqrt{\frac{2W_S}{\rho g^2}}\hat{t} \qquad x = \frac{2W_S}{\rho g}\hat{x} \qquad v = \sqrt{\frac{2W_S}{\rho}}\hat{v} \qquad a = g\hat{a} \tag{2.5}$$

The time, length, and velocity, and acceleration scales are thus

$$T = \sqrt{\frac{2W_S}{\rho g^2}} \qquad L = \frac{2W_S}{\rho g} \qquad \frac{L}{T} = \sqrt{\frac{2W_S}{\rho}} \qquad \frac{L}{T^2} = g \tag{2.6}$$

3 Velocity polar diagram when C_L and C_D are constant

When the lift and drag coefficients are constants, only stable equilibria are possible. Additionally, they are of spiral type when the lift-to-drag ratio is less that 0.354. Below is a velocity polar diagram constructed using lift and drag coefficients values report in Socha *et. al* (2010), table 1, for one configuration used in their simulations. We use 'Case 6: Average' with $C_L = .54$, $C_D = .29$, and $C_L/C_D = 1.88$. They also proposed a definition of equilibrium based on when the glide angle reaches 5% of its asymptotic value; this range is also indicated on the velocity polar diagram.

As is clear, there is strong spiraling behavior around a stable focus equilibrium point. As indicated in figure 3 in the main text, this equilibrium point is far from the boundary between a node and a focus. Additionally, the velocity polar diagram indicates that all initial conditions will lead to a stable glide and that the low acceleration magnitude region is confined around the equilibrium point.

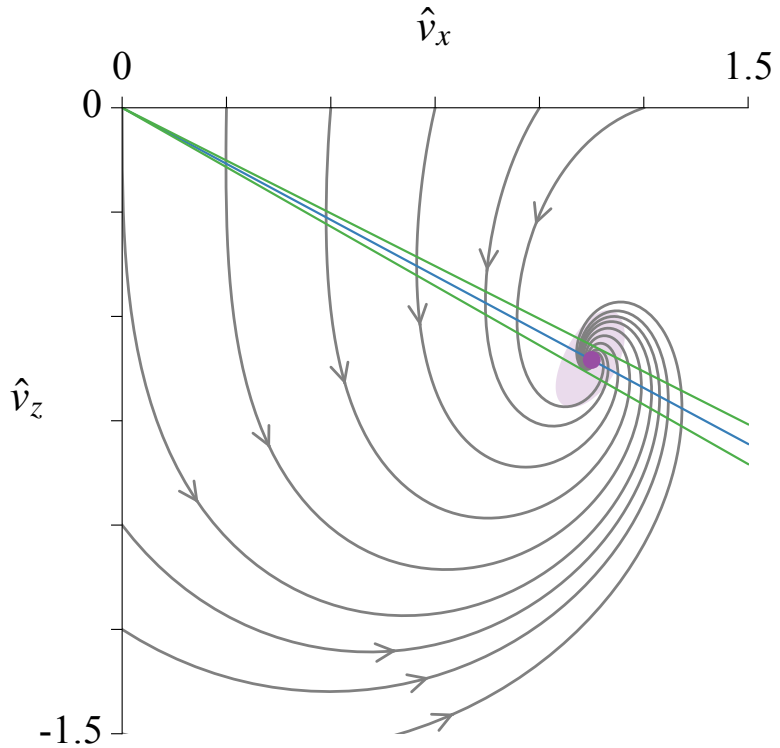

Figure 1: Velocity polar diagram for constant lift and drag coefficients. The equilibrium condition proposed by Socha *et. al* (2010).

4 Kinematic lift and drag coefficient curves

Here we derive the lift and drag force from the horizontal and vertical forces. The lift and drag force are then used to calculate the lift and drag coefficients. We beginning with the horizontal and vertical forces:

$$F_x = ma_x = F_L \sin\gamma - F_D \cos\gamma$$
$$F_z = ma_z = F_L \cos\gamma + F_D \sin\gamma - mg$$

To calculate the lift force, we multiply the x-equation by $\sin\gamma$ and the z-equation by $\cos\gamma$ and sum. This gives

$$\begin{aligned} F_x \sin\gamma + F_z \cos\gamma =& F_L(\sin^2\gamma + \cos^2\gamma) + \\ & F_D(\cos\gamma \sin\gamma - \cos\gamma \sin\gamma) - mg\cos\gamma, \end{aligned}$$

which simplifies to

$$F_L = F_x \sin\gamma + F_z \cos\gamma + mg\cos\gamma.$$

To obtain the drag force, we multiply the x-equation by $-\cos\gamma$ and the z-equation by $\sin\gamma$ and sum. This gives

$$\begin{aligned} -F_x \cos\gamma + F_z \sin\gamma =& F_L(\cos\gamma \sin\gamma - \cos\gamma \sin\gamma) + \\ & F_D(\sin^2\gamma + \cos^2\gamma)) - mg\sin\gamma, \end{aligned}$$

which simplifies to,

$$F_D = -F_x \cos\gamma + F_z \sin\gamma + mg\sin\gamma.$$

The lift and drag coefficients become

$$C_L(\gamma + \theta_b) = \frac{ma_x \sin\gamma + ma_z \cos\gamma + mg\cos\gamma}{\frac{1}{2}\rho v^2 S}$$
$$C_D(\gamma + \theta_b) = \frac{-ma_x \cos\gamma + ma_z \sin\gamma + mg\sin\gamma}{\frac{1}{2}\rho v^2 S}$$

The lift and drag coefficients have been written with explicit dependence on both glide angle and body pitch angle θ_b. The glide angle is calculated at each measurement location as $\gamma = -\tan^{-1} v_z/v_x$, but the body pitch angle is not accessible from the kinematics data and must be estimated throughout the entire glide. The body pitch angle was specified to be 0° such that the animal is horizontal to the ground. Short glides presented in [1] of *Glaucomys volans* showed a pitch angle tending towards 0°.

Individual squirrel glide trials presented in the data supplement of [2] were reanalyzed for this study. The data set consists of 59 glides of wild northern flying squirrel (*Glaucomys sabrinus*). A

majority of trials, 23 of 59, landed on a tree 18 m from the launch site. We analyze these glides because they were analyzed in detail by in ref. [2] and because longer glides give more opportunity to reach equilibrium. Individual squirrels were not marked, so analyses were performed using an average size squirrel based on previous studies. Therefore, we are calculating 'equivalent' lift and drag curves.

Of the 18 m glides, we further restrict the data set to 14 trajectories based on the start and end positions. We require the initial recorded position to be within 3.8 m horizontally and 2 m vertically from the jump point. We also require the trajectories to end with a horizontal distance between 16 m to 18.5 m. These values were selected to ensure the longest possible glides and to capture as much of the transient portion as possible. Note that most of the ballistic phase of the trajectory was not recorded in the original data set.

Velocities and accelerations are calculated using a moving window procedure similar to [2]. Velocities are calculated by iterating through the individual position components and fitting a linear polynomial to the window. The derivative of the window polynomial is evaluated at the current time to calculate velocity. Acceleration was calculated in a similar way, using the velocity time series as input. A half-window is used at the start and end of each time series. The half-window grows until it reaches the set window size. The variable window size increased derivative scatter if a higher-order polynomial was used. This was especially noticeable at the end of the trajectory where reported digitzation errors are largest. For all trials, a total window of 81 points, or 0.64 sec, was used. This window uses 40 points before and after the current time step. A large interrogation window was used to obtain the bulk glide performance and smooth out small corrections to the trajectory [2]. Lift and drag coefficient curves were calculated as described above, as was the lift-to-drag ratio. There was significant scatter in the lift and drag curves at small glide angles and therefore angles of attack. This occurred late in the glide, where digitization error was highest. We therefore restricted these curves to start at 10°, and performed glide angle binning from 10° to 44° in 2° increments. Next, a third-order spline was fit to the individual lift and drag coefficient curves. The scatter and binning is shown in figure 2.

Mean kinematic lift-to-drag ratio curves were calculated by aggregating all glide trials for a particular species. Because glide angle varied continuously during glides, points within a defined glide angle range were averaged. A Taylor moment expansion was used to find the mean and variance of the lift-to-drag-ratio [3, 4]. Naively taking the ratio of lift coefficient to drag coefficient will result in a biased ratio. We use a Taylor series expansion to find the mean and variance of the lift-to-drag ratio in each glide angle bin using

$$
\begin{aligned}
E\left[\frac{C_L(\alpha_b)}{C_D(\alpha_b)}\right] &\approx E\left[\frac{C_L(\alpha_b)}{C_D(\alpha_b)}\right] - \frac{\mathrm{cov}[C_L(\alpha_b), C_D(\alpha_b)]}{E[C_D(\alpha_b)]^2} + \frac{E[C_L(\alpha_b)]}{E[C_D(\alpha_b)]^3}\mathrm{var}[C_D(\alpha_b)] \\
\mathrm{var}\left[\frac{C_L(\alpha_b)}{C_D(\alpha_b)}\right] &\approx \frac{\mathrm{var}[C_L(\alpha_b)]}{E[C_D(\alpha_b)]^2} - \frac{2E[C_L(\alpha_b)]}{E[C_D(\alpha_b)]^3}\mathrm{cov}[C_L(\alpha_b), C_D(\alpha_b)] \\
&\quad + \frac{E[C_L(\alpha_b)]^2}{E[C_D(\alpha_b)]^4}\mathrm{var}[C_D(\alpha_b)]
\end{aligned}
$$

where $\alpha_b = \gamma + \theta_b$ and $\text{cov}[C_L(\alpha_b), C_D(\alpha_b)]$ is the covariance.

Although the kinematic method of determining aerodynamic coefficients is not ideal, it does provide a measure of the coefficient curves of gliders in their natural setting. Similar techniques have been used for small fixed-wing gliders [5, 6] where multiple markers were placed on the glider, position data differentiated, and aerodynamic parameter calculated. However, this is an idealization of the experimental data available here, including the mass distribution of animal gliders, unsteady fluid mechanics, varying wing size and shape, and time-varying mass distribution.

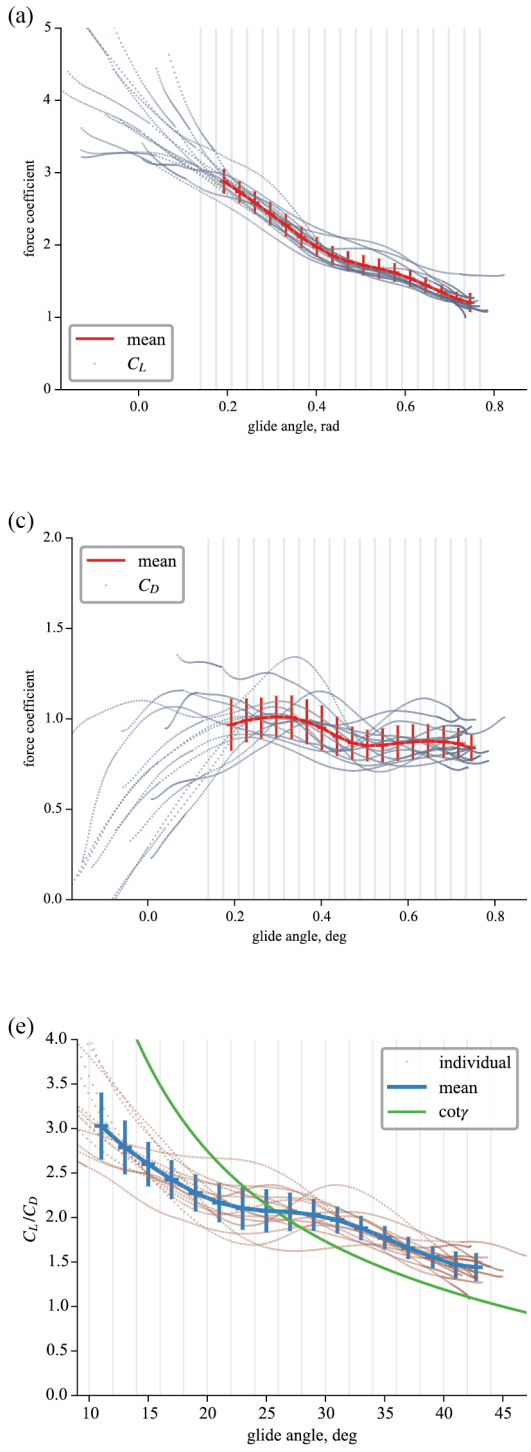

Figure 2: Mean kinematics-based lift, drag, and lift-to-drag ratio coefficient curves.

5 Numerical implementation of Velocity Polar Diagrams

Velocity polar diagrams are constructed by integrating the Cartesian equations of motion for initial conditions $(\hat{v}_{0,x}, \hat{v}_{0,z})$ along the perimeter of the velocity space. This technique requires 1) spline fits of the lift and drag coefficients, 2) the measured angle of attack range, and 3) the specified pitch angle of the glider. The horizontal and vertical velocity initial conditions are specified such that $\alpha_{\min} < \gamma_0 - \theta < \alpha_{\max}$, where $\gamma_0 = -\tan^{-1} \hat{v}_{0,z}/\hat{v}_{0,x}$. This results in the wedge shape of some velocity polar diagrams. Trajectories are found by integrating the equations forward in time using a variable time step fifth-order accurate Dormand-Prince ODE solver until one of the following conditions is met: the angle of attack exceeded the experimentally recorded range; the solver integrates for a total non-dimensional time of 30; or the velocity trajectory leaves the bounding box $\hat{v}_x \in [0, 1.25]$, $\hat{v}_z \in [0, -1.25]$. Each trajectory is then plotted to show the phase space flow.

Equilibrium points are found as described in the main text and plotted on the velocity polar diagram. The stable and unstable branches (separatrices) of saddle point equilibria are found by integrating trajectories forward and backwards in time for four initial conditions surrounding the saddle, offset by ± 0.0001. The backwards integration identifies the unstable branches and the forward integration specifies the stable branches. Finally, low acceleration regions and nullclines are found by evaluating the Cartesian equations of motion on a fine grid and then plotting contour plots for the following conditions: $|a| < 0.1$ and $\hat{v}_z' = 0$.

6 Stability Analysis and Terminal Velocity Manifold Computation

Below we list the analytical calculation of the terminal velocity manifold and details about the Hopf bifurcation.

The equilibrium condition implies

$$\begin{aligned}
\bar{v}^* &= \frac{1}{\left(C_L(\alpha^*)^2 + C_D(\alpha^*)^2\right)^{1/4}} \\
\gamma^* &= \cot^{-1}\left(\frac{C_L(\alpha^*)}{C_D(\alpha^*)}\right) \\
\bar{v}_x^* &= \quad \bar{v}^* \cos\gamma^* \\
\bar{v}_z^* &= -\bar{v}^* \sin\gamma^* \\
\alpha^* &= \theta + \gamma^*
\end{aligned}$$

6.1 Expansion about the equilibrium

In order to obtain an analytical approximation of the eigenvalues and eigenvectors, and to put the system in a form where we can analytically obtain the glide manifold in the snake phase space, we first do a change of coordinates centered on an equilibrium point. We will work in polar coordinates,

since the equations of motion look simpler,

$$\psi = \gamma - \gamma^*, \qquad r = \bar{v} - \bar{v}^* \tag{6.1}$$

where we are working in non-dimensional and rescaled variables. At equilibrium we know

$$\begin{aligned} \hat{v}' = 0 &\Rightarrow \bar{v}^{*2} C_D(\alpha) = \sin\gamma^* \\ \gamma' = 0 &\Rightarrow \bar{v}^{*2} C_L(\alpha) = \cos\gamma^*. \end{aligned} \tag{6.2}$$

In the shifted coordinates, the equilibrium is the origin and the equations of motion are

$$\begin{aligned} \psi' &= -(\bar{v}^* + r) C_L(\gamma^* + \theta^* + \varphi + \psi) + \frac{1}{(\bar{v}^* + r)} \cos(\gamma^* + \psi), \\ r' &= -(\bar{v}^* + r)^2 C_D(\gamma^* + \theta^* + \varphi + \psi) + \sin(\gamma^* + \psi), \end{aligned} \tag{6.3}$$

We want to write the right-hand-side of the equations of motion as a power series expansion in ψ and r. To start out, we will get this expansion to second-order.

Let's first look at the ψ' expression. Note that, via Taylor expansion,

$$\frac{1}{(\bar{v}^* + r)} = \frac{1}{\bar{v}^* \left(1 + \frac{r}{\bar{v}^*}\right)} = \frac{1}{\bar{v}^*} \left(1 - \frac{r}{\bar{v}^*} + \left(\frac{r}{\bar{v}^*}\right)^2 - \left(\frac{r}{\bar{v}^*}\right)^3 + \mathcal{O}\left(\frac{r}{\bar{v}^*}\right)^4\right) \tag{6.4}$$

Using the cos addition formula,

$$\cos(\gamma^* + \psi) = \cos\psi \cos\gamma^* - \sin\psi \sin\gamma^* \tag{6.5}$$

along with (6.2), we get

$$\begin{aligned} \frac{1}{\bar{v}^*} \cos(\gamma^* + \psi) &= \frac{1}{\bar{v}^*} \left[\bar{v}^{*2} C_L(\alpha^*) \cos\psi - \bar{v}^{*2} C_D(\alpha^*) \sin\psi\right] \\ &= \bar{v}^* \left[C_L(\alpha^*) \cos\psi - C_D(\alpha^*) \sin\psi\right] \end{aligned} \tag{6.6}$$

so,

$$\begin{aligned} \frac{1}{(\bar{v}^* + r)} \cos(\gamma^* + \psi) &= \bar{v}^* \left[C_L(\alpha^*) \cos\psi - C_D(\alpha^*) \sin\psi\right] \left(1 - \frac{r}{\bar{v}^*} + \left(\frac{r}{\bar{v}^*}\right)^2 - \left(\frac{r}{\bar{v}^*}\right)^3 + \mathcal{O}\left(\frac{r}{\bar{v}^*}\right)^4\right) \\ &= \bar{v}^* \left[C_L(\alpha^*) \cos\psi - C_D(\alpha^*) \sin\psi\right] - r \left[C_L(\alpha^*) \cos\psi - C_D(\alpha^*) \sin\psi\right] \\ &+ \left(\frac{r^2}{\bar{v}^*} - \frac{r^3}{\bar{v}^{*2}}\right) \left[C_L(\alpha^*) \cos\psi - C_D(\alpha^*) \sin\psi\right] + \mathcal{O}\left(r^4\right) \end{aligned} \tag{6.7}$$

Also note that $C_L(\gamma^* + \theta^* + \varphi + \psi) = C_L(\alpha^* + \psi)$, and by Taylor series expansion we have

$$C_L(\alpha^* + \psi) = C_L(\alpha^*) + \psi C_L'(\alpha^*) + \tfrac{1}{2}\psi^2 C_L''(\alpha^*) + \mathcal{O}(\psi^3) \tag{6.8}$$

and similarly for the drag term,

$$C_D(\alpha^* + \psi) = C_D(\alpha^*) + \psi C_D'(\alpha^*) + \tfrac{1}{2}\psi^2 C_D''(\alpha^*) + \tfrac{1}{6}\psi^3 C_D'''(\alpha^*) + \mathcal{O}(\psi^4) \tag{6.9}$$

so,

$$\begin{aligned} -(\bar{v}^* + r)C_L(\gamma^* + \theta^* + \varphi + \psi) = &-\bar{v}^* \left[C_L(\alpha^*) + \psi C_L'(\alpha^*) + \tfrac{1}{2}\psi^2 C_L''(\alpha^*) + \tfrac{1}{6}\psi^3 C_D'''(\alpha^*) + \mathcal{O}(\psi^4)\right] \\ &- r\left[C_L(\alpha^*) + \psi C_L'(\alpha^*) + \tfrac{1}{2}\psi^2 C_L''(\alpha^*) + \mathcal{O}(\psi^3)\right] \end{aligned} \tag{6.10}$$

So the ψ' expression becomes

$$\begin{aligned} \psi' = &\bar{v}^* \left(-C_L(\alpha^* + \psi) + C_L(\alpha^*)\cos\psi - C_D(\alpha^*)\sin\psi\right) \\ &+ r\left(-C_L(\alpha^* + \psi) - C_L(\alpha^*)\cos\psi + C_D(\alpha^*)\sin\psi\right) \\ &+ \left(\frac{r^2}{\bar{v}^*} - \frac{r^3}{\bar{v}^{*2}}\right)\left[C_L(\alpha^*)\cos\psi - C_D(\alpha^*)\sin\psi\right] + \mathcal{O}\left(r^4\right) \end{aligned} \tag{6.11}$$

Note the Taylor series up to 3rd order in ψ for cos and sin is,

$$\cos\psi = 1 - \tfrac{1}{2}\psi^2 + \mathcal{O}(\psi^4), \qquad \sin\psi = \psi - \tfrac{1}{6}\psi^3 + \mathcal{O}(\psi^5)$$

Plugging in all the Taylor series expansions, we get, up through 3rd order in ψ and r,

$$\begin{aligned} \psi' = &\bar{v}^* \left(-C_L - \psi C_L' - \tfrac{1}{2}\psi^2 C_L'' - \tfrac{1}{6}\psi^3 C_D''' + C_L - \tfrac{1}{2}\psi^2 C_L - \psi C_D + \tfrac{1}{6}\psi^3 C_D\right) \\ &+ r\left(-C_L - \psi C_L' - \tfrac{1}{2}\psi^2 C_L'' - C_L + \tfrac{1}{2}\psi^2 C_L + C_D\psi\right) \\ &+ \left(\frac{r^2}{\bar{v}^*} - \frac{r^3}{\bar{v}^{*2}}\right)\left[C_L - C_D\psi\right] + \mathcal{O}\left(4\right) \end{aligned} \tag{6.12}$$

where it should be understood that the lift and drag coefficients and all their derivatives (w.r.t. angle of attack) are evaluated at the critical point α^*, and where $\mathcal{O}(4)$ stands for terms which are fourth order or higher in the variables ψ and r.

Grouping terms by powers in ψ and r, we get

$$\begin{aligned} \psi' = &\bar{v}^* \left[-C_L' - C_D\right]\psi + 2\left[-C_L\right] r \\ &+ \tfrac{\bar{v}^*}{2}\left[-C_L'' - C_L\right]\psi^2 + \left[-C_L' + C_D\right]\psi r + \tfrac{1}{\bar{v}^*}[C_L]r^2 \\ &+ \tfrac{\bar{v}^*}{6}[C_D - C_L''']\psi^3 + \tfrac{1}{2}[C_L - C_L'']\psi^2 r + \tfrac{1}{\bar{v}^*}[-C_D]\psi r^2 + \tfrac{1}{\bar{v}^{*2}}[-C_L]r^3 + \mathcal{O}(4) \end{aligned} \tag{6.13}$$

There are terms linear in ψ and r, terms second-order in ψ and r, and terms third-order in ψ and r.

We can follow a similar procedure for the r' expression. Using the sin addition formula,

$$\sin(\gamma^* + \psi) = \sin\psi\cos\gamma^* + \cos\psi\sin\gamma^* \tag{6.14}$$

along with (6.2), we get

$$\begin{aligned}\sin(\gamma^* + \psi) &= \left[\bar{v}^{*2} C_L \sin\psi + \bar{v}^{*2} C_D \cos\psi\right] \\ &= \bar{v}^{*2}\left[C_L \sin\psi + C_D \cos\psi\right] \\ &= \bar{v}^{*2}\left[C_L\psi - \tfrac{1}{6}C_L\psi^3 + C_D - \tfrac{1}{2}\psi^2 C_D + \mathcal{O}(4)\right]\end{aligned} \tag{6.15}$$

Also,

$$\begin{aligned}-(\bar{v}^* + r)^2 C_D(\alpha^* + \psi) = &-\bar{v}^{*2}\left[C_D + \psi C_D' + \tfrac{1}{2}\psi^2 C_D'' + \tfrac{1}{6}\psi^3 C_D''' + \mathcal{O}(4)\right] \\ &- 2\bar{v}^* r\left[C_D + \psi C_D' + \tfrac{1}{2}\psi^2 C_D'' + \mathcal{O}(3)\right] \\ &- r^2\left[C_D + \psi C_D' + \mathcal{O}(2)\right]\end{aligned} \tag{6.16}$$

so we get

$$\begin{aligned}r' = &\bar{v}^{*2}\left[-C_D' + C_L\right]\psi + 2\left[-\bar{v}^* C_D\right] r \\ &+ \tfrac{\bar{v}^{*2}}{2}\left[-C_D - C_D''\right]\psi^2 + 2\bar{v}^*[-C_D']\psi r + [-C_D] r^2 \\ &+ \tfrac{\bar{v}^{*2}}{6}[-C_L - C_D''']\psi^3 + \bar{v}^*[-C_D'']\psi^2 r + \tfrac{1}{2}[-C_D']\psi r^2 + [0] r^3 + \mathcal{O}(4)\end{aligned} \tag{6.17}$$

Putting the (ψ, r) system into matrix form, we have

$$\begin{bmatrix}\psi' \\ r'\end{bmatrix} = \underbrace{\begin{bmatrix}\bar{v}^*\left[-C_L' - C_D\right] & [-2C_L] \\ \bar{v}^{*2}\left[-C_D' + C_L\right] & [-2\bar{v}^* C_D]\end{bmatrix}}_{\mathbf{A}} \begin{bmatrix}\psi \\ r\end{bmatrix} + \mathbf{F}(\psi, r) + \mathcal{O}(4) \tag{6.18}$$

where $\mathbf{F}(\psi, r)$ stands for second and third-order terms, and is given by

$$\mathbf{F}(\psi, r) = \begin{bmatrix}F^1(\psi, r) \\ F^2(\psi, r)\end{bmatrix} \tag{6.19}$$

where

$$\begin{aligned}F^1(\psi, r) = &\tfrac{\bar{v}^*}{2}\left[-C_L - C_L''\right]\psi^2 + \left[C_D - C_L'\right]\psi r + \tfrac{1}{\bar{v}^*}[C_L] r^2 \\ &+ \tfrac{\bar{v}^*}{6}[C_D - C_L''']\psi^3 + \tfrac{1}{2}[C_L - C_L'']\psi^2 r + \tfrac{1}{\bar{v}^*}[-C_D]\psi r^2 + \tfrac{1}{\bar{v}^{*2}}[-C_L] r^3\end{aligned} \tag{6.20}$$

and

$$\begin{aligned}F^2(\psi, r) = &\tfrac{\bar{v}^{*2}}{2}\left[-C_D - C_D''\right]\psi^2 + 2\bar{v}^*[-C_D']\psi r + [-C_D] r^2 \\ &+ \tfrac{\bar{v}^{*2}}{6}[-C_L - C_D''']\psi^3 + \bar{v}^*[-C_D'']\psi^2 r + \tfrac{1}{2}[-C_D']\psi r^2 + [0] r^3\end{aligned} \tag{6.21}$$

From the 2×2 linearization matrix $\mathbf{A}$ in (6.18),

$$\mathbf{A} = \begin{bmatrix}\bar{v}^*\left[-C_L' - C_D\right] & [-2C_L] \\ \bar{v}^{*2}\left[-C_D' + C_L\right] & [-2\bar{v}^* C_D]\end{bmatrix} \tag{6.22}$$

(also given in appendix A), we can analytically determine the eigenvalues and eigenvectors in terms of the equilibrium point and characteristics of the lift and drag curves at that point.

For this simple system, we can write the eigenvalue equation in the standard form as [7, p. 130]

$$\lambda^2 - \bar{\tau}\lambda + \bar{\Delta} = 0,$$

where $\bar{\tau} = \text{trace}(\mathbf{A})$ and $\bar{\Delta} = \det(\mathbf{A})$. The eigenvalues are

$$\lambda_1 = \frac{\bar{\tau} + \sqrt{\bar{\tau}^2 - 4\bar{\Delta}}}{2}, \qquad \lambda_2 = \frac{\bar{\tau} - \sqrt{\bar{\tau}^2 - 4\bar{\Delta}}}{2}$$

The trace of $\mathbf{A}$ is

$$\bar{\tau} = \bar{v}^* \left[-C_L' - 3C_D\right]$$

and the determinant of $\mathbf{A}$ is

$$\bar{\Delta} = 2\bar{v}^{*2} \left[C_L^2 + C_D^2 + C_L' C_D - C_D' C_L\right]$$

So,

$$\begin{aligned} \bar{\tau}^2 - 4\bar{\Delta} &= \bar{v}^{*2} \left[(C_L' + 3C_D)^2 - 8(C_L^2 + C_D^2 + C_L' C_D - C_D' C_L)\right] \\ &= \bar{v}^{*2} \left[C_L'^2 + C_D^2 - 2C_L' C_D - 8C_L^2 + 8C_D' C_L\right] \\ &= \bar{v}^{*2} \left[(C_D - C_L')^2 - 8C_L(C_L - C_D')\right] \end{aligned} \tag{6.23}$$

and the eigenvalues are

$$\lambda_{1,2} = \frac{\bar{\tau} \pm \sqrt{\bar{\tau}^2 - 4\bar{\Delta}}}{2}$$

We can write the eigenvalues more compactly by introducing τ and Δ,

$$\begin{aligned} \tau &= (C_L'/C_D) + 3 \\ \Delta &= (C_L/C_D)' + (C_L/C_D)^2 + 1 \end{aligned} \tag{6.24}$$

such that

$$\begin{aligned} \bar{\tau} &= -\frac{C_D}{(C_L^2 + C_D^2)^{1/4}}\tau \\ \bar{\Delta} &= 2\frac{C_D^2}{(C_L^2 + C_D^2)^{1/2}}\Delta \end{aligned} \tag{6.25}$$

in which case,

$$\lambda_{1,2} = \frac{C_D}{2(C_L^2 + C_D^2)^{1/4}} \left(-\tau \pm \sqrt{\tau^2 - 8\Delta}\right) \tag{6.26}$$

and since the prefactor

$$\frac{C_D}{2(C_L^2 + C_D^2)^{1/4}} \tag{6.27}$$

is always a positive scalar, the location of the eigenvalues on the complex plane is given solely by τ and Δ.

6.2 Hopf bifurcation case

We often view the pitch variable θ as a bifurcation parameter. A Hopf bifurcation occurs when $\bar{\tau} = 0$ and $\bar{\Delta} > 0$, so the eigenvalues are purely imaginary,

$$\lambda_{\pm} = \pm i\omega$$

where $\omega = \sqrt{\bar{\Delta}} > 0$. Suppose this occurs along the branch of equilibria at a particular value of θ which we'll call $\bar{\theta}$. By the assumption of $\bar{\tau} = 0$, we conclude that

$$C_L' = -3C_D \tag{6.28}$$

and from $\bar{\Delta} > 0$, we conclude that

$$C_L > \tfrac{1}{2}\left(C_D' + \sqrt{C_D'^2 + 8C_D^2}\right) \quad \text{or} \quad \mathrm{C_L} < \tfrac{1}{2}\left(\mathrm{C_D'} - \sqrt{\mathrm{C_D'^2 + 8C_D^2}}\right) \tag{6.29}$$

Notice that the sign of

$$d = \frac{d}{d\theta}\left(\mathrm{Re}(\lambda(\theta))\right)\Big|_{\theta=\bar{\theta}} = \tfrac{1}{2}\bar{\tau}' = \tfrac{1}{2}\bar{v}^*(-C_L'' - 3C_D') \tag{6.30}$$

is an indication of the type of bifurcation. If, as θ increases, the equilibrium point is going from a stable to unstable focus, then $\bar{\tau}' > 0$. Otherwise, $\bar{\tau}' < 0$. Note that

$$\begin{aligned} C_L'' &< -3C_D' \quad \text{going from stable to unstable}, \bar{\tau}' > 0 \\ C_L'' &> -3C_D' \quad \text{going from unstable to stable}, \bar{\tau}' < 0 \end{aligned} \tag{6.31}$$

For the case of purely imaginary eigenvalues, we have

$$\mathbf{A} = \begin{bmatrix} \bar{v}^* 2C_D & -2C_L \\ \bar{v}^{*2}\left(-C_D' + C_L\right) & -\bar{v}^* 2C_D \end{bmatrix} \tag{6.32}$$

where the eigenvalues are $\pm i\omega$, where

$$\omega = \bar{v}^*\sqrt{2}\sqrt{C_L^2 - C_L C_D' - 2C_D^2} \tag{6.33}$$

is positive. We solve for the generalized eigenvectors $\mathbf{u}$ and $\mathbf{v}$,

$$\mathbf{u} = \begin{bmatrix} 2C_L \\ \bar{v}^* 2C_D \end{bmatrix} \quad \mathbf{v} = \begin{bmatrix} 0 \\ \omega \end{bmatrix} \tag{6.34}$$

Define the matrix $\mathbf{P}$ as

$$\mathbf{P} = [\mathbf{u} \;\; \mathbf{v}]$$

so $\mathbf{u}$ is the first column of $\mathbf{P}$ and $\mathbf{v}$ is the second column of $\mathbf{P}$. This matrix defines a linear transformation to the eigenbasis (x, y) via

$$\begin{bmatrix} \psi \\ r \end{bmatrix} = \mathbf{P} \begin{bmatrix} x \\ y \end{bmatrix}$$

so the x coordinate is along the $\mathbf{u}$ direction and the y coordinate is along the $\mathbf{v}$ direction. Note that

$$\begin{aligned} \psi &= 2C_L x \\ r &= \bar{v}^* 2C_D x + \omega y \end{aligned} \tag{6.35}$$

The dynamics in the eigenbasis are

$$\begin{bmatrix} x' \\ y' \end{bmatrix} = \begin{bmatrix} 0 & -\omega \\ \omega & 0 \end{bmatrix} \begin{bmatrix} x \\ y \end{bmatrix} + \mathbf{P}^{-1}\mathbf{F}(2C_L x, \bar{v}^* 2C_D x + \omega y) + \mathcal{O}(4) \tag{6.36}$$

where $\mathbf{F}$, from (6.19), includes the 2nd and 3rd order terms and where

$$\mathbf{P}^{-1} = \begin{bmatrix} \frac{1}{2C_L} & 0 \\ -\frac{\bar{v}^* C_D}{\omega C_L} & \frac{1}{\omega} \end{bmatrix} \tag{6.37}$$

We will re-write the nonlinear terms, defining $\mathbf{f}(x, y) = \mathbf{P}^{-1}\mathbf{F}(2C_L x, \bar{v}^* 2C_D x + \omega y)$, so the resulting equation now has the form,

$$\begin{bmatrix} x' \\ y' \end{bmatrix} = \begin{bmatrix} 0 & -\omega \\ \omega & 0 \end{bmatrix} \begin{bmatrix} x \\ y \end{bmatrix} + \begin{bmatrix} f^1(x, y) \\ f^2(x, y) \end{bmatrix} \tag{6.38}$$

The coefficient a, from [8] and [9], which determines what kind of Hopf bifurcation will occur, can be calculated as

$$\begin{aligned} a = &\tfrac{1}{16}\left[f^1_{xxx} + f^1_{xyy} + f^2_{xxy} + f^2_{yyy}\right] \\ &+ \tfrac{1}{16\omega}\left[f^1_{xy}(f^1_{xx} + f^1_{yy}) - f^2_{xy}(f^2_{xx} + f^2_{yy}) - f^1_{xx}f^2_{xx} + f^1_{yy}f^2_{yy}\right] \end{aligned} \tag{6.39}$$

where all partial derivatives are evaluated at the bifurcation point, $\theta = \bar{\theta}$, $x = 0$, $y = 0$,

$$\begin{aligned}
F^1_{xx} &= \bar{v}^*(4{C_L}^3 - 4{C_L}^3 C''_L + 36 C_L {C_D}^2) \\
F^1_{xy} &= \omega 12 C_L C_D \\
F^1_{yy} &= \bar{v}^* 4 C_L({C_L}^2 - C_L C'_D - 2{C_D}^2) \\
F^2_{xx} &= -\bar{v}^{*2}(4{C_L}^2 C_D + 8{C_D}^3 + 4{C_L}^2 C''_D + 16 C_L C_D C'_D) \\
F^2_{xy} &= -\bar{v}^* \omega(C_L C'_L + {C_D}^2) \\
F^2_{yy} &= -\bar{v}^{*2} 4 C_D({C_L}^2 - C_L C'_D - 2{C_D}^2) \\
F^1_{xxx} &= -\bar{v}^*(8{C_L}^3 C'''_L + 24{C_L}^2 C_D C''_L + 96 C_L {C_D}^3 - 32{C_L}^3 C_D) \\
F^1_{xyy} &= -\bar{v}^* 32 C_D C_L({C_L}^2 - C_L C'_D - 2{C_D}^2) \\
F^1_{xxy} &= \bar{v}^*(4[C_L - C''_L]{C_L}^2(\tfrac{\omega}{\bar{v}^*}) - 40 C_L {C_D}^2(\tfrac{\omega}{\bar{v}^*})) \\
F^1_{yyy} &= -\bar{v}^* 12 C_L({C_L}^2 - C_L C'_D - 2{C_D}^2)(\tfrac{\omega}{\bar{v}^*}) \\
F^2_{xxy} &= -\bar{v}^* \omega(8{C_L}^2 C''_D + 8 C_L C_D C'_D) \\
F^2_{yyy} &= 0
\end{aligned} \tag{6.40}$$

and we get the partial derivatives of $\mathbf{f}(x, y)$ from the relationship

$$\mathbf{f}(x, y) = \mathbf{P}^{-1}\mathbf{F}(x, y)$$

which give us

$$\begin{aligned}
f^1(x, y) &= \tfrac{1}{2C_L} F_1(x, y) \\
f^2(x, y) &= -\tfrac{\bar{v}^* C_D}{\omega C_L} F_1(x, y) + \tfrac{1}{\omega} F_2(x, y)
\end{aligned} \tag{6.41}$$

Knowing the sign of a along with the sign of τ' will determine which of the four cases of Hopf bifurcation is present, via the Poincaré-Andronov-Hopf Bifurcation Theorem ([8]).

For example, for the pitch bifurcation diagram of the 'kinematic squirrel', we see a Hopf bifurcation for a critical $\bar{\theta}$ near 0. We can see that $d < 0$ (eigenvalues going from right half-plane to left half-plane as $\theta - \bar{\theta}$ increases through zero). The numerically determined unstable limit cycle exists for $\theta > \bar{\theta}$, which is consistent with $a > 0$, so we predict that calculating (6.39) will give $a > 0$. We also predict that the limit cycle will have a period of approximately $T = \frac{2\pi}{\omega}$ where ω is given from (6.33), and that the radius of the limit cycle in the (x, y) plane, close to the pitch value $\bar{\theta}$, is given by

$$\rho = \sqrt{-\tfrac{d}{a}(\theta - \bar{\theta})} \tag{6.42}$$

Notice that the dependence of ρ on the constants a and d, as well as distance away from the bifurcation point, $(\theta - \bar{\theta})$, reveal how 'quickly' the size of the limit cycle grows. The amplitude of

the limit cycle in terms of glide angle γ is provided from (6.35) as,

$$\rho_\gamma = 2C_L\rho = 2C_L\sqrt{-\tfrac{d}{a}(\theta - \bar{\theta})} \tag{6.43}$$

6.3 Stable node case

If $\bar{\tau} < 0$ and $\bar{\tau}^2 - 4\bar{\Delta} > 0$ (so $\sqrt{\bar{\tau}^2 - 4\bar{\Delta}} > 0$), then we have two real, and negative, eigenvalues. The larger magnitude eigenvalue is

$$\lambda_{ss} = \frac{\bar{\tau} - \sqrt{\bar{\tau}^2 - 4\bar{\Delta}}}{2} = \tfrac{1}{2}\bar{v}^* \left(-C_L' - 3C_D - \sqrt{(C_D - C_L')^2 - 8C_L(C_L - C_D')} \right), \tag{6.44}$$

and the smaller magnitude eigenvalue is

$$\lambda_s = \frac{\bar{\tau} + \sqrt{\bar{\tau}^2 - 4\bar{\Delta}}}{2} = \tfrac{1}{2}\bar{v}^* \left(-C_L' - 3C_D + \sqrt{(C_D - C_L')^2 - 8C_L(C_L - C_D')} \right), \tag{6.45}$$

so $\lambda_{ss} < \lambda_s < 0$, where '$s$' denotes *stable* and '$ss$' denotes *super stable*. Let the corresponding eigenvectors be $\mathbf{e}_{ss}$ and $\mathbf{e}_s$, respectively, understood as column vectors.

Now $\bar{\tau} < 0$ implies that

$$C_L' > -3C_D$$

, and $\bar{\tau}^2 - 4\bar{\Delta} > 0$ implies that

$$(C_D - C_L')^2 > 8C_L(C_L - C_D')$$

We can solve for $\mathbf{e}_s$, since it will give us a local approximation of the *terminal velocity manifold* described in the text. All we want is the slope $\bar{m}$ (in (ψ, r) coordinates), so we let $\mathbf{e}_s = [-1, -\bar{m}]^T$. From the eigenvector formula

$$\mathbf{A}\mathbf{e}_s = \lambda_s \mathbf{e}_s$$

where

$$\mathbf{A} = \begin{bmatrix} a & b \\ c & d \end{bmatrix} \tag{6.46}$$

we have

$$\bar{m} = \frac{\lambda_s - a}{b} \tag{6.47}$$

and using (6.22) and (6.53), we get

$$a = \bar{v}^* \left[-C_L' - C_D \right], \quad b = [-2C_L]$$

and thus,

$$\bar{m} = \frac{\bar{v}^*}{4C_L} \left(C_D - C_L' - \sqrt{(C_D - C_L')^2 - 8C_L(C_L - C_D')} \right) \tag{6.48}$$

We want the slope m in $(\bar{v}_x, \bar{v}_z)$ coordinates, so, using the relationship between the cartesian and polar coordinates,

$$\begin{aligned} \bar{v}_x &= \quad \bar{v}\cos\gamma \\ \bar{v}_z &= -\bar{v}\sin\gamma \end{aligned}$$

we write the transformation between local vectors,

$$\begin{bmatrix} d\bar{v}_x \\ d\bar{v}_z \end{bmatrix} = \begin{bmatrix} -\bar{v}^*\sin\gamma^* & \cos\gamma^* \\ -\bar{v}^*\cos\gamma^* & -\sin\gamma^* \end{bmatrix} \begin{bmatrix} d\psi \\ dr \end{bmatrix} \tag{6.49}$$

and letting $dr = \bar{m}\, d\psi$, we get the slope of the terminal velocity manifold,

$$m = \frac{d\bar{v}_z}{d\bar{v}_x} = \frac{\bar{v}^*\cos\gamma^* + \bar{m}\sin\gamma^*}{\bar{v}^*\sin\gamma^* - \bar{m}\cos\gamma^*} \tag{6.50}$$

with $\bar{m}$ as in (6.56). Note, this is the *local* slope of the terminal velocity manifold, as evaluated at the stable node point. The slope may change, i.e., the manifold may be curved, as explored in the next case.

For completeness, we also compute the eigenvector $\mathbf{e}_{ss} = [-1, -\bar{n}]^T$, and get

$$\bar{n} = \frac{\bar{v}^*}{4C_L}\left(C_D - C_L' + \sqrt{(C_D - C_L')^2 - 8C_L(C_L - C_D')}\right) \tag{6.51}$$

6.4 Saddle case

If $\bar{\Delta} < 0$, so $\bar{\Delta} = -|\bar{\Delta}|$, then $\sqrt{\bar{\tau}^2 - 4\bar{\Delta}} = \sqrt{\bar{\tau}^2 + 4|\bar{\Delta}|} > |\bar{\tau}|$, then we have two real eigenvalues, one negative (λ_s) and one positive (λ_u). The negative eigenvalue is

$$\lambda_s = \frac{\bar{\tau} - \sqrt{\bar{\tau}^2 - 4\bar{\Delta}}}{2} = \tfrac{1}{2}\bar{v}^*\left(-C_L' - 3C_D - \sqrt{(C_D - C_L')^2 - 8C_L(C_L - C_D')}\right), \tag{6.52}$$

and the positive eigenvalue is

$$\lambda_u = \frac{\bar{\tau} + \sqrt{\bar{\tau}^2 - 4\bar{\Delta}}}{2} = \tfrac{1}{2}\bar{v}^*\left(-C_L' - 3C_D + \sqrt{(C_D - C_L')^2 - 8C_L(C_L - C_D')}\right), \tag{6.53}$$

Let the corresponding eigenvectors be $\mathbf{e}_s$ and $\mathbf{e}_u$, respectively, understood as column vectors.

We can solve for $\mathbf{e}_u$, since it will give us a local approximation of the *terminal velocity manifold* described in the text. All we want is the slope $\bar{m}$ (in (ψ, r) coordinates), so we let $\mathbf{e}_u = [-1, -\bar{m}]^T$. From the eigenvector formula

$$\mathbf{A}\mathbf{e}_u = \lambda_u \mathbf{e}_u$$

where

$$\mathbf{A} = \begin{bmatrix} a & b \\ c & d \end{bmatrix} \tag{6.54}$$

we have

$$\bar{m} = \frac{\lambda_u - a}{b} \tag{6.55}$$

and using (6.22) and (6.53), we get

$$a = \bar{v}^* \left[-C_L' - C_D \right], \quad b = [-2C_L]$$

and thus,

$$\bar{m} = \frac{\bar{v}^*}{4C_L} \left(C_D - C_L' - \sqrt{(C_D - C_L')^2 - 8C_L(C_L - C_D')} \right) \tag{6.56}$$

We want the slope m in $(\bar{v}_x, \bar{v}_z)$ coordinates, so, using the relationship between the cartesian and polar coordinates,

$$\begin{aligned} \bar{v}_x &= \quad \bar{v} \cos\gamma \\ \bar{v}_z &= -\bar{v} \sin\gamma \end{aligned} \tag{6.57}$$

we write the transformation between local vectors,

$$\begin{bmatrix} d\bar{v}_x \\ d\bar{v}_z \end{bmatrix} = \begin{bmatrix} -\bar{v}^* \sin\gamma^* & \cos\gamma^* \\ -\bar{v}^* \cos\gamma^* & -\sin\gamma^* \end{bmatrix} \begin{bmatrix} d\psi \\ dr \end{bmatrix} \tag{6.58}$$

and letting $dr = \bar{m}\, d\psi$, we get the slope of the terminal velocity manifold,

$$m = \frac{d\bar{v}_z}{d\bar{v}_x} = \frac{\bar{v}^* \cos\gamma^* + \bar{m} \sin\gamma^*}{\bar{v}^* \sin\gamma^* - \bar{m} \cos\gamma^*} \tag{6.59}$$

with $\bar{m}$ as in (6.56). Again, this is the *local* slope of the terminal velocity manifold, as evaluated at the saddle point, and may be different from the local slope of the terminal velocity manifold as evaluated at the stable node, if the manifold is curved.

For completeness, we also compute the eigenvector $\mathbf{e}_s = [-1, -\bar{n}]^T$, and get

$$\bar{n} = \frac{\bar{v}^*}{4C_L} \left(C_D - C_L' + \sqrt{(C_D - C_L')^2 - 8C_L(C_L - C_D')} \right) \tag{6.60}$$

Higher order approximation of terminal velocity manifold. Define the matrix $\mathbf{P}$ as

$$\begin{aligned} \mathbf{P} &= [\mathbf{e}_u \;\; \mathbf{e}_s] \\ &= \begin{bmatrix} -1 & -1 \\ -\bar{m} & -\bar{n} \end{bmatrix} \end{aligned}$$

so $\mathbf{e}_u$ is the first column of $\mathbf{P}$ and $\mathbf{e}_s$ is the second column of $\mathbf{P}$.

This matrix defines a linear transformation to the eigenbasis (x, y) via

$$\begin{bmatrix} \psi \\ r \end{bmatrix} = \mathbf{P} \begin{bmatrix} x \\ y \end{bmatrix}$$

so the x coordinate is along the $\mathbf{e}_u$ direction and the y coordinate is along the $\mathbf{e}_s$ direction. Note that

$$\begin{aligned} \psi &= -x - y \\ r &= -\bar{m}x - \bar{n}y \end{aligned} \tag{6.61}$$

and

$$\mathbf{P}^{-1} = \frac{1}{\bar{m} - \bar{n}} \begin{bmatrix} \bar{n} & -1 \\ -\bar{m} & 1 \end{bmatrix} \tag{6.62}$$

Considering (6.18), we have

$$\begin{bmatrix} x' \\ y' \end{bmatrix} = \underbrace{\mathbf{P}^{-1}\mathbf{A}\mathbf{P}}_{\mathbf{\Lambda}} \begin{bmatrix} x \\ y \end{bmatrix} + \mathbf{P}^{-1}\mathbf{F}(x, y) \tag{6.63}$$

where $\mathbf{\Lambda}$ is the diagonalized matrix,

$$\mathbf{\Lambda} = \begin{bmatrix} \lambda_u & 0 \\ 0 & \lambda_s \end{bmatrix}$$

and where care must be taken to calculate the second-order terms, $\mathbf{P}^{-1}\mathbf{F}(x, y)$, in terms of x and y, where $\mathbf{F}(x, y)$ is given as in (6.19)-(6.21).

We will re-write the nonlinear terms, defining $\mathbf{f}(x, y) = \mathbf{P}^{-1}\mathbf{F}(-x - y, -\bar{m}x - \bar{n}y)$, so

$$\mathbf{f}(x, y) = \frac{1}{\bar{m} - \bar{n}} \begin{bmatrix} \bar{n} & -1 \\ -\bar{m} & 1 \end{bmatrix} \begin{bmatrix} a_1x^2 + a_2xy + a_3y^2 \\ b_1x^2 + b_2xy + b_3y^2 \end{bmatrix} + \mathcal{O}(3)$$

where

$$
\begin{aligned}
a_1 &= a^1 + b^1\bar{m} + c^1\bar{m}^2 \\
a_2 &= 2a^1 + b^1(\bar{m} + \bar{n}) + 2c^1\bar{m}\bar{n} \\
a_3 &= a^1 + b^1\bar{n} + c^1\bar{n}^2 \\
b_1 &= a^2 + b^2\bar{m} + c^2\bar{m}^2 \\
b_2 &= 2a^2 + b^2(\bar{m} + \bar{n}) + 2c^2\bar{m}\bar{n} \\
b_3 &= a^2 + b^2\bar{n} + c^2\bar{n}^2 \\
a^1 &= \tfrac{\bar{v}^*}{2}\left[-C_L - C_L''\right] \\
b^1 &= \left[C_D - C_L'\right] \\
c^1 &= \tfrac{1}{\bar{v}^*}[C_L] \\
a^2 &= \tfrac{\bar{v}^{*2}}{2}\left[-C_D - C_D''\right] \\
b^2 &= 2\bar{v}^*[-C_D'] \\
c^2 &= [-C_D]
\end{aligned}
$$

We will refer to the components of $\mathbf{f}$ as (f, g).

The resulting equation now has the form,

$$
\begin{bmatrix} x' \\ y' \end{bmatrix} = \begin{bmatrix} \lambda_u & 0 \\ 0 & \lambda_s \end{bmatrix} \begin{bmatrix} x \\ y \end{bmatrix} + \begin{bmatrix} f(x,y) \\ g(x,y) \end{bmatrix} \tag{6.64}
$$

where

$$
\begin{aligned}
f(x,y) &= c_1x^2 + c_2xy + c_3y^2 + \mathcal{O}(3) \\
g(x,y) &= d_1x^2 + d_2xy + d_3y^2 + \mathcal{O}(3)
\end{aligned} \tag{6.65}
$$

where

$$
\begin{aligned}
c_i &= \tfrac{1}{\bar{m}-\bar{n}}(\ \ \bar{n}a_i - b_i) \\
d_i &= \tfrac{1}{\bar{m}-\bar{n}}(-\bar{m}a_i + b_i)
\end{aligned}
$$

We will end up with the expansion about the equilibrium in a form where we can now calculate the terminal velocity manifold. We re-write (6.64) as,

$$
\begin{aligned}
x' &= \lambda_u x + f(x,y) \\
y' &= \lambda_s y + g(x,y)
\end{aligned} \tag{6.66}
$$

where $f(x, y)$ is second-order and higher in x and y, as is $g(x, y)$.

We assume the terminal velocity manifold is given by $y = h(x)$, where $h(x)$ has the Taylor series

expansion form,

$$h(x) = ax^2 + bx^3 + \mathcal{O}(x^4) \tag{6.67}$$

We can solve for the coefficients a and b by taking the time derivative of $y = h(x)$, which gives

$$\frac{\partial h}{\partial x} x' - y' = 0$$

i.e.,

$$\frac{\partial h}{\partial x} \left[\lambda_u x + f(x, h(x))\right] - \left[\lambda_s h(x) + g(x, h(x))\right] = 0$$

and equating like powers of x,

$$(2ax + 3bx^2 + \mathcal{O}(x^3)) \left[\lambda_u x + c_1 x^2 + \mathcal{O}(x^3)\right] - \left[\lambda_s a x^2 + d_1 x^2 + \mathcal{O}(x^3)\right] = 0$$

i.e.,

$$\left[a(2\lambda_u - \lambda_s) - d_1\right] x^2 = 0$$

so

$$a = \frac{d_1}{(2\lambda_u - \lambda_s)}$$

Thus, to a second-order approximation in the (x, y) coordinates, the terminal velocity manifold is expressed as

$$y = h(x) = \frac{d_1}{(2\lambda_u - \lambda_s)} x^2 + \mathcal{O}(x^3)$$

thus, in general the manifold will be curved. To get the curvature up through third-order terms, we need b, so we would have to have $\mathbf{f}(x, y)$ calculated up to the third-order terms. We note that this whole process can be automated using automatic power series expansion tools [10].

To get the terminal velocity manifold in the original $(\bar{v}_x, \bar{v}_z)$ coordinates, we use (6.61), (6.1), and (6.57), to get a parametric curve,

$$\begin{aligned} \bar{v}_x(u) = &\quad (\bar{v}^* - \bar{m}u - \bar{n}h(u)) \cos(\gamma^* - u - h(u)) \\ \bar{v}_z(u) = &-(\bar{v}^* - \bar{m}u - \bar{n}h(u)) \sin(\gamma^* - u - h(u)) \end{aligned} \tag{6.68}$$

parametrized by a curvilinear coordinate u which we take to be in some interval $I \subset \mathbb{R}$, where the function h is as in (6.67).

We can determine the lowest order non-linear approximation of the vector field *along the 1-dimensional terminal velocity manifold*, as

$$\begin{aligned} u' &= \lambda_u u + f(u, h(u)) \\ &= \lambda_u u + c_1 u^2 + \mathcal{O}(u^3) \end{aligned} \tag{6.69}$$

where we are using u as a curvilinear (arc-length) coordinate along the terminal velocity manifold. This is the analytical formula for the 'speed' (actually, acceleration) along the terminal velocity

curve vs. location along that curve. This tells us that a second equilibrium point (stable) will show up along the terminal velocity manifold at $u = -\lambda_u/c_1$, which is an approximation of where the stable node is located.

It is interesting that the local approximation of the dynamics around the saddle point can imply the existence of the stable point. Also noteworthy is the fact that the terminal velocity manifold constructed from the saddle point to the stable node is a heteroclinic trajectory (backward asymptotic to the saddle point and forward asymptotic to the stable node) along which the relative speed varies according to (6.69).

To find out what role the shape of the terminal velocity manifold plays in modifying the vector field along it, we must consider third-order terms in (6.18), which would give us

$$\begin{aligned} u' &= \lambda_u u + f_2(u, h(u)) + f_3(u, h(u)) + \mathcal{O}(u^4) \\ &= \lambda_u u + c_1 u^2 + c_2 a u^3 + k_1 u^3 + \mathcal{O}(u^4) \\ &= \lambda_u u + c_1 u^2 + \left[c_2 \tfrac{d}{(2\lambda_u - \lambda_s)} + k_1 \right] u^3 + \mathcal{O}(u^4) \end{aligned} \tag{6.70}$$

where $f_2(x, y) = c_1 x^2 + c_2 xy + c_3 y^2$ and $f_3(x, y) = k_1 x^3 + k_2 x^2 y + k_3 x y^2 + k_4 y^3$ are the second and third order terms in the x' equation of (6.66), respectively.

Note that

$$k_1 = \tfrac{1}{\bar{m} - \bar{n}} (\bar{n} \tilde{a}_1 - \tilde{b}_1)$$

where

$$\begin{aligned} \tilde{a}_1 &= -(A_1 + A_2 \bar{m} + A_3 \bar{m}^2 + A_4 \bar{m}^3) \\ \tilde{b}_1 &= -(B_1 + B_2 \bar{m} + B_3 \bar{m}^2 + B_4 \bar{m}^3) \end{aligned}$$

and where the A_i and B_i come from the third-order coefficients in (6.20) and (6.21), respectively,

$$\begin{aligned} A_1 &= \tfrac{\bar{v}^*}{6} [C_D - C_L'''] \\ A_2 &= \tfrac{1}{2} [C_L - C_L''] \\ A_3 &= \tfrac{1}{\bar{v}^*} [-C_D] \\ A_4 &= \tfrac{1}{\bar{v}^{*2}} [-C_L] \\ B_1 &= \tfrac{\bar{v}^{*2}}{6} [-C_L - C_D'''] \\ B_2 &= \bar{v}^* [-C_D''] \\ B_3 &= \tfrac{1}{2} [-C_D'] \\ B_4 &= 0 \end{aligned}$$

We note that the third-order coefficient b is given by

$$b = \frac{g_1 - a(2c_1 - d_2)}{3\lambda_u - \lambda_s}$$

where

$$g_1 = \frac{1}{\bar{m}-\bar{n}}(-\bar{m}\tilde{a}_1 + \tilde{b}_1)$$

6.5 Terminal velocity manifold as slow manifold

In the previous sections, we have looked for local approximations of the terminal velocity manifold near an equilibrium point, building off of the invariant manifold structure near the equilibrium. However, we may be able to consider another, more global approach, inspired by singular perturbation theory [7]. In some systems, one can identify a fast variable and a slow variable when a small parameter appears in one of the ODEs. The dynamics of the fast variable quickly collapse onto a lower dimensional manifold on which the dynamics evolve more slowly (the slow variable). In the re-scaled gliding equations of motion for $(\bar{v}_x, \bar{v}_z)$, no slow-fast structure can be identified in the equations themselves (i.e., there is no natural choice of a small parameter), yet a slow manifold appears to exist. While we do not consider it here, there may methods to obtain the approximate slow manifold [11, 12], based on the extended zero derivative principle, even if fast and slow variables have not been identified.

6.6 Acceleration along the terminal velocity manifold

In figure 5bii of the text, we include an inset showing the approximation of the terminal velocity manifold in the vicinity of the saddle point equilibrium. Below we show the acceleration magnitude of the glider along the manifold using both the 2^{nd}-order and 3^{rd}-order approximations.

References

[1] Kristin L Bishop. The relationship between 3-D kinematics and gliding performance in the southern flying squirrel, *Glaucomys volans*. *J. Exp. Biol.*, 209:689–701, 2006. doi: 10.1242/jeb.02062.

[2] Joseph W. Bahlman, Sharon M. Swartz, Daniel K. Riskin, and Kenneth S. Breuer. Glide performance and aerodynamics of non-equilibrium glides in northern flying squirrels (*Glaucomys sabrinus*). *J. R. Soc. Interface*, 10(20120794), 2013. doi: 10.1098/rsif.2012.0794.

[3] Haym Benaroya, Seon Mi Han, and Mark Nagurka. *Probability Models in Engineering and Science*, volume 193. CRC Press, 2005.

[4] Alex Papanicolaou. Taylor approximation and the delta method, 2009.

[5] B. F. Mettler. Extracting micro air vehicles aerodynamic forces and coefficients in free flight using visual motion tracking techniques. *Exp. Fluids*, 49:557–569, 2010. doi: 10.1007/s00348-009-0803-6.

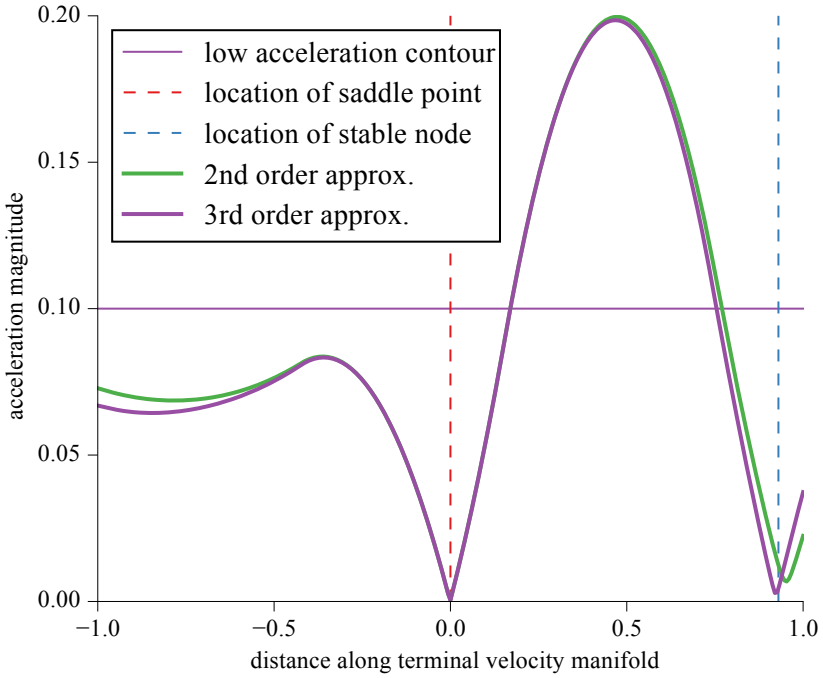

Figure 3: Acceleration along the terminal velocity manifold for the airfoil snake at a pitch angle of $\theta = 5°$

.

[6] Daniel V. Uhlig and Michael S. Selig. Determining aerodynamic characteristics of a micro air vehicle using motion tracking. *J. Aircr.*, 50:1481–1490, 2013. doi: 10.2514/1.C031996.

[7] Steven H. Strogatz. *Nonlinear Dynamics and Chaos: With Applications to Physics, Biology, Chemistry, and Engineering*. Perseus Books Publishing, LLC, 2001.

[8] Stephen Wiggins. *Introduction to Applied Nonlinear Dynamical Systems and Chaos*, volume 2. Springer Science & Business Media, 2003.

[9] J.E. Marsden and M. McCracken. *The Hopf Bifurcation and Its Applications*. Springer-Verlag, New York, Heidelberg, Berlin, 1976.

[10] G. Gómez, W. S. Koon, M. W. Lo, J. E. Marsden, J. Masdemont, and S. D. Ross. Connecting orbits and invariant manifolds in the spatial three-body problem. *Nonlinearity*, 17:1571–1606, 2004.

[11] Morten Brøns. An iterative method for the canard explosion in general planar systems. *Discrete and Continuous Dynamical Systems Supplement 2013*, pages 77–83, 2013.

[12] M. Brøns and K. Uldall Kristiansen. On the approximation of the canard explosion point in epsilon-free systems. *ArXiv e-prints*, 2015.